



CHORUS

This is the accepted manuscript made available via CHORUS. The article has been published as:

Structure functions in nocturnal atmospheric boundary layer turbulence

Eliezer Kit, Eli Barami, and H. J. S. Fernando

Phys. Rev. Fluids **6**, 084605 — Published 17 August 2021

DOI: [10.1103/PhysRevFluids.6.084605](https://doi.org/10.1103/PhysRevFluids.6.084605)

Structure Functions in Nocturnal Atmospheric Boundary Layer Turbulence

Kit Eliezer^{1,3*}, Barami Eli^{2,4}, Fernando HJS^{3,5}

¹ School of Mechanical Engineering, Tel Aviv University, Tel Aviv 69978; Israel,
elikit@gmail.com

² Department of Mechanical Engineering, Ben-Gurion University of the Negev, Beer-Sheva,
84105, Israel

³ Department of Civil and Environmental Engineering and Earth Sciences, University of Notre
Dame, Notre Dame, IN 46530

⁴ Soreq Nuclear Research Center, Yavne 8180000 Israel

⁵ Department of Aerospace and Mechanical Engineering, University of Notre Dame, Notre
Dame, IN 46530

* Corresponding author: elikit@gmail.com; Tel.: +972-3-6408-929

Abstract: This paper analyzes odd and even higher order moments for longitudinal velocity increment $\Delta u(x, r)$, where x is the longitudinal coordinate and r the separation distance, based on the canonical and a new (modified) normalization for skewness of longitudinal velocity derivative $\partial u / \partial x$. Two types of data were used, stably stratified turbulence data from nocturnal Atmospheric Boundary Layer taken during the MATERHORN field campaign and from the Direct Numerical Simulation (DNS) of homogeneous and isotropic turbulence in a box at four Reynolds numbers and four different grid resolution. Third moment data normalized by the same moment of third order for modulus $|\Delta u(x, r)|$ representing modified skewness of velocity increment showed a better collapse at all Reynolds numbers in the *inertial* and *viscous* sub-ranges than canonical normalized skewness with normalization parameter $\langle (\Delta u(x, r))^2 \rangle^{3/2}$, where $\langle \cdot \rangle$ representing the ensemble average. The analysis also considered odd p^{th} order classical structure functions $\langle \Delta u(x, r)^p \rangle$ with Kolmogorov-theory based normalization $\langle \Delta u(x, r)^p \rangle / (\varepsilon r)^{p/3}$ for the *inertial* subrange, where ε is the rate of dissipation, and a modulus-based structure function $\langle |\Delta u(x, r)|^p \rangle / (\varepsilon r)^{p/3}$. Both types of structure functions of order $p = (1 \div 6)$ were computed using different normalizations, and corresponding scaling exponents were assessed for the *inertial* and *viscous* sub-ranges. Scaling for modulus-based structure functions in the *viscous* sub-range was identified as $|\Delta u(x, r)|^p \propto r^{p g(5/6)}$. In the *viscous* sub-range, the velocity increment varied linear with r for the classical third moment $\langle \Delta u(x, r)^3 \rangle \propto r^3$ based on velocity increment while the classical fifth moment

$\langle \Delta u(x, r)^5 \rangle$ did not provide any meaningful scaling exponent. A plausible qualitative explanation linking these effects to anisotropy of nocturnal stratified turbulence is proposed.

Keywords: Structure Function, High order moments, Direct Numerical Simulation (DNS), Intermittency; Bursting; Probability Density Function (PDF), Skewness

1. Introduction

In his seminal work, Kolmogorov [K41, 1] proposed two hypotheses/postulates on turbulence:

1. Kolmogorov Self-Similarity Hypothesis (KSSH), which enabled to express, based on dimensionless considerations, the structure function $L_p(r)$ defined as a moment of any order p of the velocity increment Δu at a separation r as a function of ε (mean turbulent kinetic energy TKE dissipation rate) and r as $L_p(r) = (\Delta u)^p \propto (r\varepsilon)^{p/3}$. This is strictly appropriate for Homogeneous Isotropic Turbulence (HIT), a theoretical abstraction that can be made pragmatic by introducing the Postulate of Local Isotropy (PLI) as below.

2. PLI assumes that far from boundaries and external forces applied at large scales, turbulence loses memory as it cascades down from large to smaller scales, wherein turbulence becomes locally isotropic and therefore KSSH is applicable. This cascading region (inertial subrange) is suitably separated from the regions of larger TKE containing scales and much smaller viscous dissipation scales. The dissipation subrange is also locally isotropic, but viscous influence therein engenders scaling laws different from those of the inertial subrange.

In most subsequent studies the KSSH was tested for the inertial subrange, and an anomalous exponent instead of the Kolmogorov $p/3$ scaling was observed. To explain and predict such anomalies, a large number of models have been suggested, for example, Extended Self Similarity Hypothesis (ESSH), Refined KSSH (RKSH) and fractal models. Most of them included the intermittency, especially that of ε . There is strong evidence from field, laboratory and direct numerical simulation (DNS) studies to suggest that ε is associated with small-scale turbulence structures distributed unevenly in space, being confined to a smaller fraction of space determined by the size of small eddies [2, 3], thus undermining KSSH [1]. As such, it is well known that the scaling exponents differ dramatically from the Kolmogorov $p/3$ exponents, and this disparity increases with both p and r^{-1} [4], revealing non-Gaussian behavior [5] in HIT. As well, real turbulent flows include anisotropic forcing and boundary conditions, particularly in stratified fluids

[6, 7, 8], and this anisotropy may penetrate to *inertial* and, perhaps, *dissipation/viscous* sub-ranges. This perfusion of anisotropy obviously puts PLI into question, as discussed below.

Literature of DNS studies on HIT at high Taylor microscale Reynolds numbers Re_λ , e.g. [9, 10, 11] are voluminous. Benzi et al. [12, 13] experimentally investigated scaling laws using grid flows and at the center of jet and wake flows. Extended Self Similarity (ESS) based on the use of third order structure function for normalization instead of separation r was applied to determine anomalous scaling exponents; significant anomalies were observed, in good agreement with peer studies. Instead of third order longitudinal structure function $L_3(r) = \langle (\Delta u(x, r))^3 \rangle$, an alternative function $L_3^*(r) = \langle |\Delta u(x, r)|^3 \rangle$ was proposed [12, 13, 14]. As expected in the *viscous* sub-range for very small normalized separations $r/\eta \approx 1$, where η is the Kolmogorov scale, the velocity difference $\Delta u(x, r)$ is regular, causing both the velocity difference and its modulus to be approximately proportional to r . Similar results were obtained by the same group [15, 16] and others [17 - 23]. Most efforts by Benzi et al. [15, 16] and She & Leveque [19] were focused on identifying the most appropriate model for anomalous scaling exponents.

Sreenivasan et al.'s [24] measurements in the surface layer of the atmospheric boundary layer (ABL) reached very high Taylor microscale Reynolds numbers Re_λ (10,000 to 20,000), but PLI could not be validated, which was ascribed to the presence of mean shear. Laboratory experiments with homogeneous shear flow by Warhaft and his co-workers [25-27] showed unambiguously that return to isotropy expected at small scales does not occur either at lower $Re_\lambda \sim O(100)$ [25] or at higher Re_λ numbers $\sim O(1000)$ [26], which again was ascribed to shear. To quote [26] "The results show that PLI is untenable, both at the dissipation and inertial scales, at least to $R_\lambda \sim 1000$, and suggest it is unlikely to be so even at higher Reynolds numbers." In grid flows without shear [30], however, the isotropy at small scales could be realized, and thus the expected praxis of zero odd transversal structure functions was manifested.

Effects of shear on similarity laws, scaling laws, intermittency and anisotropy of small scales have been further studied in laboratory experiments and DNS of Channel Flow Turbulence, Wall Bounded Turbulence, Homogeneous Shear Flows, and Nonhomogeneous Turbulence [28-34]. With regards to similarity laws, in HIT the celebrated KSSH was replaced by Refined Kolmogorov Similarity Hypothesis (RKSH) [5] to account for intermittency of ε , which was found appropriate and sound away from the wall (logarithmic) region of the boundary layer. Near the wall, where shear is strong, the classical RKSH was not valid, and an 'alternative RKSH' [29] has been

proposed to account for stronger intermittency. Therein, PLI at small scales was violated as anisotropy penetrated the smallest scales, scaling anomalies become pronounced, and scaling exponents deviated from the Kolmogorov counterpart $p/3$ more remarkably than in HIT. At intermediate distances from the wall, double scaling could be obtained where both RKSH and alternative RKSH anomalous exponents appear to coexist.

In [35-40], $SO(3)$ formalism was used for systematic decomposition of structure and/or correlation functions in spherical harmonics to separate isotropic and anisotropic contributions. This decomposition enables the determination of scaling exponents in the isotropic and anisotropic sectors in the presence of strong and weak shear, thus following possible decay of anisotropic contributions at small scales. Interestingly, measurements in homogeneous shear flow by Casciola, Gualtieri, Jacob, and Piva [36,37] found that anisotropic contributions in weak shear waning at a relatively fast rate while under strong shear the anisotropy keep a significant presence up to viscous scales, thus violating PLI [37]. The latter fine-scale anisotropy is accompanied by stronger intermittency and stronger deviation of scaling exponents from HIT. These authors [37] conclude: “It has always been believed that turbulence in fluids can achieve a universal state at small scales with fluctuations that, becoming statistically isotropic, are characterized by universal scaling laws. In fact, in different branches of physics it is common to find conditions such that statistical isotropy is never recovered and the anisotropy induced by large scale shear contaminates the entire range of scales up to velocity gradients.”

Arad et al. [41] conducted ABL surface layer measurements at very high Re_λ (10,000 - 20,000), and $SO(3)$ rotation groups were employed to determine scaling exponents in different isotropic and anisotropic sectors. The contributions of anisotropic sectors were small, indicating weak effects of shear. Nevertheless, the accounting for these anisotropic contributions significantly improved the correspondence between experimental data and the analytic fit. A general theory explaining the decomposition of structure and correlation functions (by projections on the spherical harmonics) as well as determination of scaling exponents in isotropic and anisotropic sectors are presented in [42-45].

Notwithstanding above advancements with regard to shear flows, studies on possible penetration of anisotropy into small scales of stable stratified flows are far fewer. A few high-quality experimental studies [46-49] augmented by DNS [50] unambiguously show that, much the same way as for shear, strong stable stratification begets large anisotropies in the mean-squares strain rates $\partial v/\partial x$ and $\partial w/\partial x$ relative to $\partial u/\partial x$. Studies of stably stratified grid-generated HIT [46,

47] report “*an unexpected rapid onset of anisotropy in the small scales,*” which is true for *uniformly sheared thermally stratified* turbulent flow [48, 49]. A combination of shear and stratification, especially for decaying turbulence, is expected to increase the propensity for small-scale anisotropy compared due to either shear or stratification alone.

The outcomes of past research discussed above will be used in Section 3 to argue that the anomalous scaling for structure functions obtained during fine-scale hot-film measurements of turbulence in the nocturnal ABL during the field campaigns of Mountain Terrain Atmospheric Modeling and Observations (MATERHORN) Program [51, 52] is possibly due to stratification effects and not due to shear (since the measurements were conducted *well away* from the wall layer). An intriguing observation of MATERHORN was the intermittent appearance of strong bursts at nighttime (stably stratified conditions) at smaller scales characterized by ephemeral rise of velocity fluctuations and simultaneous increase of ε by orders of magnitude. The separation of data into ‘burst’ and ‘no-burst’ time intervals based on a chosen threshold of ε enabled processing of both burst and no-burst datasets independently. The dataset without bursts could follow classical Kolmogorov turbulence if the effects of stratification can be considered insignificant. The datasets with bursts behaved differently in that the TKE spectral shape exhibited bumps in the inertial sub-range [53].

This study concerns a new (modified) normalization for *higher odd moments* of longitudinal velocity increment $\Delta u(x, r)$ built upon the normalization proposed in [52] for *skewness* of the longitudinal velocity derivative $\partial u / \partial x$. No-burst datasets from MATERHORN were used along with those from limited DNS computations of HIT.

2. Methodology

An intriguing effect observed in nocturnal ABL is the appearance of episodic but puissant turbulence or ‘bursts’. Arguably, this may occur either in HIT or anisotropic turbulent flows subject to external forcing such as stratification, rotation or electromagnetic forces that promote anisotropy. These factors may magnify the deviation of the probability density functions (pdf) from Gaussian, but not necessarily increase its asymmetry present in HIT due to non-linearity. It is well known that the pdf of velocity derivatives in HIT is skewed, leading to considerable negative third moment (vis-à-vis zero for the Gaussian distribution) of longitudinal velocity derivative; this explains the appearance of generation term in the vorticity equation that causes production of enstrophy [54].

Enstrophy production and intermittency in turbulent flows occur due to two independent effects: in the HIT case, turbulence is skewed at the intermediate (inertial subrange) and small (dissipation range) scales, thus magnifying the enstrophy flux to small scales. In addition to the presence of stretched vortex sheets and vortex tubes that is associated with strong intermittency at very small scales of HIT, breaking of small-scale random internal gravity waves in (anisotropic) stably stratified turbulence may also lead to enstrophy generation and intermittency. The range of scales at which such breaking occurs and associated dynamics are yet to be understood (and the separation of internal waves from turbulence continues to be a vexing problem).

Nocturnal ABL is a case where stability evolves overnight due to radiative cooling at a pace slower than the time scale of turbulence, leading to a myriad of turbulence-related phenomena that was studied during MATERHORN (2011-2016) field experiments. A novel probing system was deployed for this purpose, the details of which are given in [52, 55]. The finer scales therein were captured with a sonic- and hot-film anemometer dyad (dubbed the ‘combo’ probe) placed on a horizontal pole at 6 m height of a 32-m high tower (labeled ES-2) equipped with an array of sonics and thermocouples at various levels. This system is described in [52] and the MATERHORN experiment in [51]. The data encompassed a variety of flow types that appear over different phases of the diurnal cycle, but careful winnowing could identify data that fit the rubric of stratified shear flows, which emerged from a katabatic flow draining from the nearby Granite Mountain.

After careful processing of sonic records of ES-2, the 90-minute period of katabatic flow starting from 22:00 MDT¹ on October 19, 2012 was selected for stratified shear flow studies. Prior to the selected time interval, the wind speed rapidly increased from ~1 m/s to ~4 m/s at the height of the combo probe. The wind direction changed from its usual oscillations before 22:00 MDT to a nearly constant direction, resembling a stratified parallel shear flow. Thereafter, the winds changed quite rapidly between 23:30 MDT and midnight [52]. Although mean quantities were quasi-steady during the selected period 22:00-23:30 MDT, careful inspection of turbulence statistics showed considerable variability. An analysis for identification of approximately homogeneous sub-intervals enabled focusing on structure function analysis in the sub-interval SI_{devd} (22:50 - 23:10 MDT). This sub-interval was considered as fully developed turbulence since flow variations were modest and appearance of bursting events were very limited (less than 2% of the time). More details can be found in [52, 56].

¹ Mountain daylight time (local time)

To augment, three-dimensional homogeneous and stationary turbulence was studied using high-resolution DNS in a periodic box with up to 1024^3 grid points. A pseudo-spectral code with large-scale random forcing and triply periodic boundary conditions was used. The white-in-time Gaussian forcing was placed in the range of scales $1 \leq k \leq \sqrt{6}$. The DNS were carried at 4 grid resolutions, yielding $Re_\lambda = 139, 201, 264, 383$. Details of the numerical scheme are given in [11].

3. Results

3.1 Datasets from Field Campaign and DNS

The datasets revealed strong bursts characterized by short-term increase of velocity fluctuations and simultaneous increase of ε by orders of magnitude. The separation between burst/no-burst time intervals was based on a threshold for ε , as in [52]. The data without bursts followed the Kolmogorov -5/3 law whereas those with bursts showed bumps in the TKE spectra. Since no-burst periods resembled Kolmogorov turbulence, it was decided to test various features of intermittency using no-burst field data sets and DNS of HIT turbulence. The analysis focused, *inter alia*, on the new (modified) normalization suggested in [53], the effects of varying Reynolds number and the scaling exponents in various sub-ranges, e.g. *inertial* and *viscous*. The new normalization is based on [53], where the second-order denominator $\left(\overline{(\partial u / \partial x)^2}\right)^{3/2}$ of the canonical skewness of the longitudinal velocity derivative $\partial u / \partial x$ is replaced by the same third order moment of its modulus $\overline{|\partial u / \partial x|^3}$ to define an alternative descriptor for intermittency studies. In our work described below, modulus based normalizations are extended for odd structure functions of higher orders $p = 3, 5, 7$.

3.2 Normalized Odd Structure Functions in DNS

The following discussion deals with longitudinal structure function $L_p(r)$ of order p ; $L_p^*(r)$ is the same function based on the absolute values of the longitudinal velocity increment $\Delta u(x, r) = u(x+r) - u(x)$, where r is the separation distance:

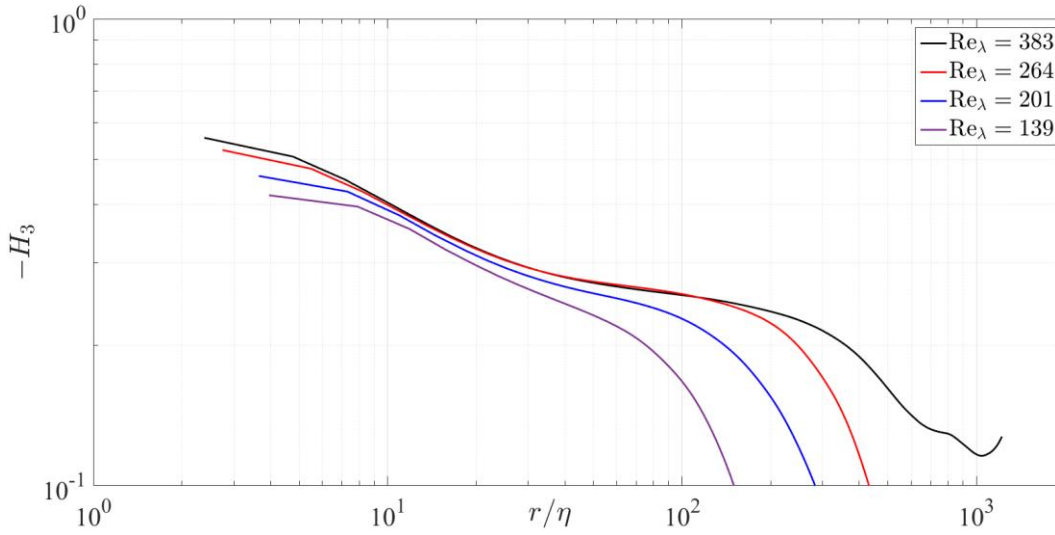
$$L_p(r) = \langle (\Delta u(x, r))^p \rangle; \quad L_p^*(r) = \langle |\Delta u(x, r)|^p \rangle. \quad (1)$$

The moments of velocity increment in the canonical form are

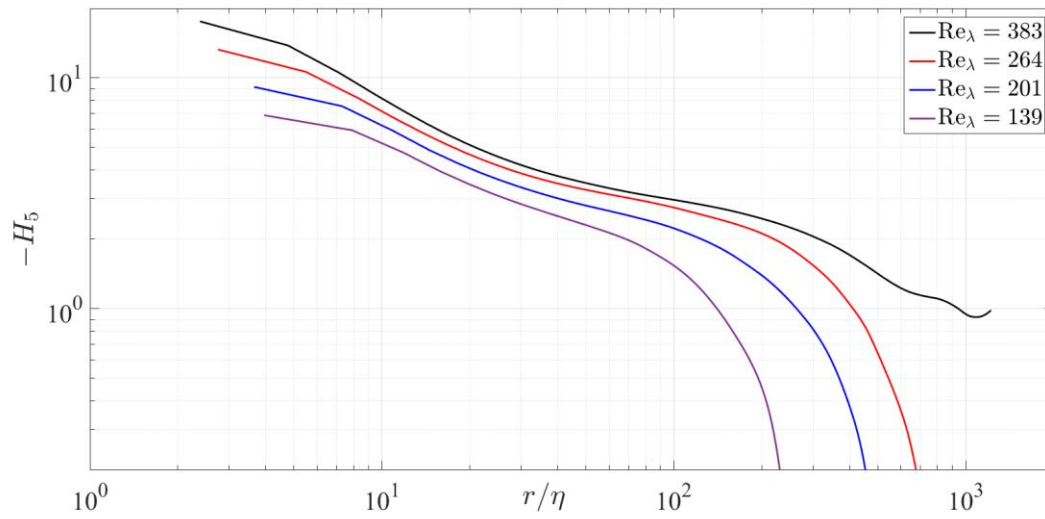
$$H_p(r) = L_p(r) / (L_2(r))^{p/2} \quad H_p^*(r) = L_p^*(r) / (L_2(r))^{p/2} \quad . \quad (2)$$

We dealt mostly with odd moments, $p = 3, 5, 7$ and, following [1], considered *modified* moments $\hat{H}_p(r) = L_p(r) / L_p^*(r) = H_p(r) / H_p^*(r)$ along with the moments obtained using *canonical* normalization presented in (2). Note that, at small separations r , the normalized structure-function based velocity *increments* become the moments of the velocity *derivative*. For example, at $p=3$, velocity derivative skewness can be retrieved as $H_3 = S = \langle (\partial u / \partial x)^3 \rangle / \langle (\partial u / \partial x)^2 \rangle^{3/2}$, which was the focus in [53].

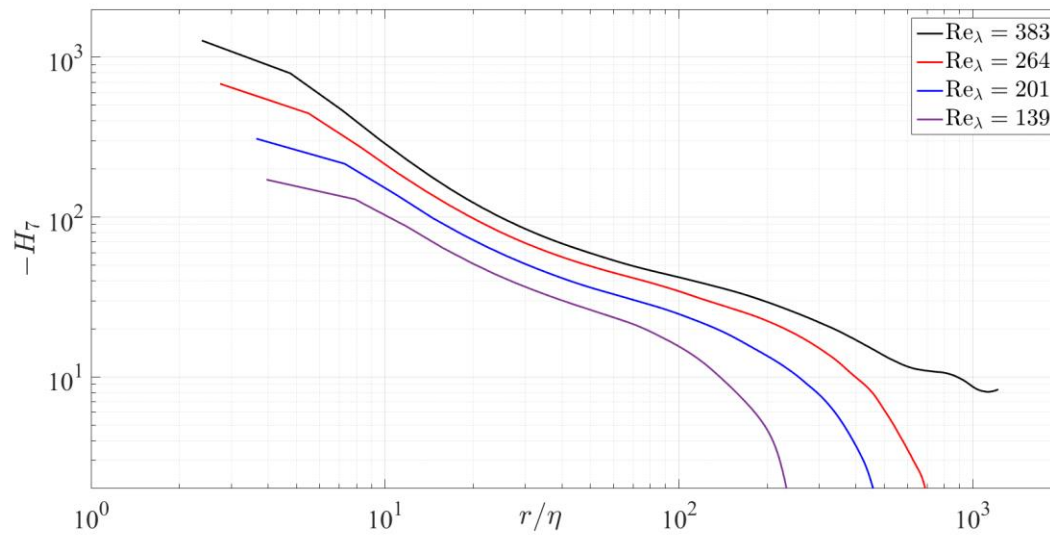
The normalized canonical moments for $p = 3, 5, 7$ at all four Re_λ numbers in DNS are given in Figure 1, and the modified moments $\hat{H}_p(r)$ for $p = 3, 5, 7$ are presented for comparison in Figure 2 where the separation scale r is normalized by the Kolmogorov length scale η .



(a)



(b)



(c)

Figure 1. Canonical odd moments for all 4 datasets obtained in DNS. (a) third, (b) fifth and (c) seventh moments.

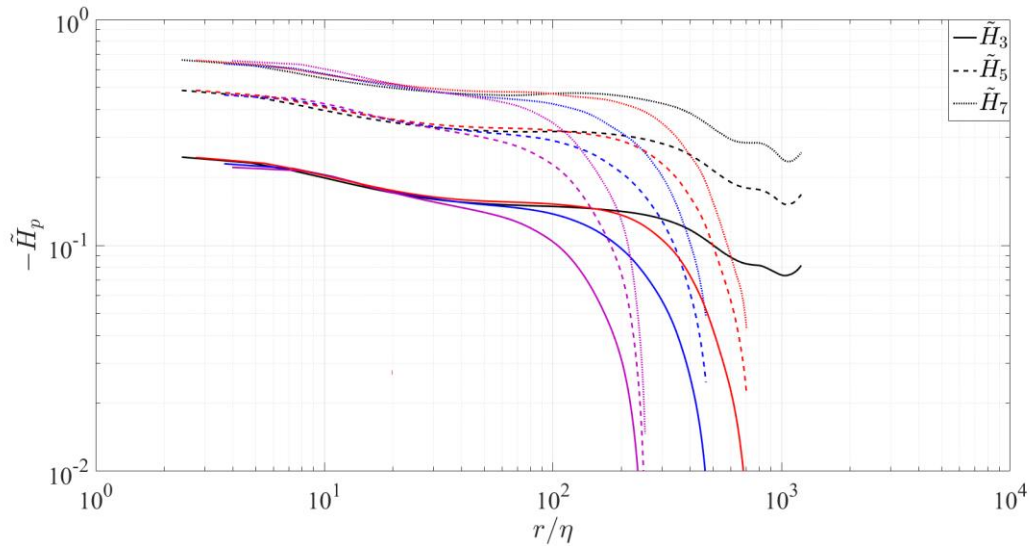


Figure 2. Modified moments for all 4 DNS datasets. Color coding is the same as in Figure 1.

Note the two striking differences between Figures 1 and 2. Plots for two highest Re_λ practically collapse in Figure 2 in both *viscous* ($r/\eta < 10$) and *inertial* ($50 \div 200$) sub-ranges while they obviously differ systematically in Figure 1 in all subranges. The upper boundary of the inertial sub-range (Figure 1) depends significantly on Re_λ and is about 300 for the highest $Re_\lambda = 383$, and it reduces remarkably at lower Re_λ due to the reduction of separation between large and dissipating scales. At larger scales, universal scaling is not expected given their dependence on boundary conditions and details of large-scale forcing. In the *inertial* sub-range, all *modified moments* (Figure 2) remain approximately constant, while *canonical moments* (Figure 1) decline with an approximately constant slope. The slope increases with the order p of moments, as was observed by [12].

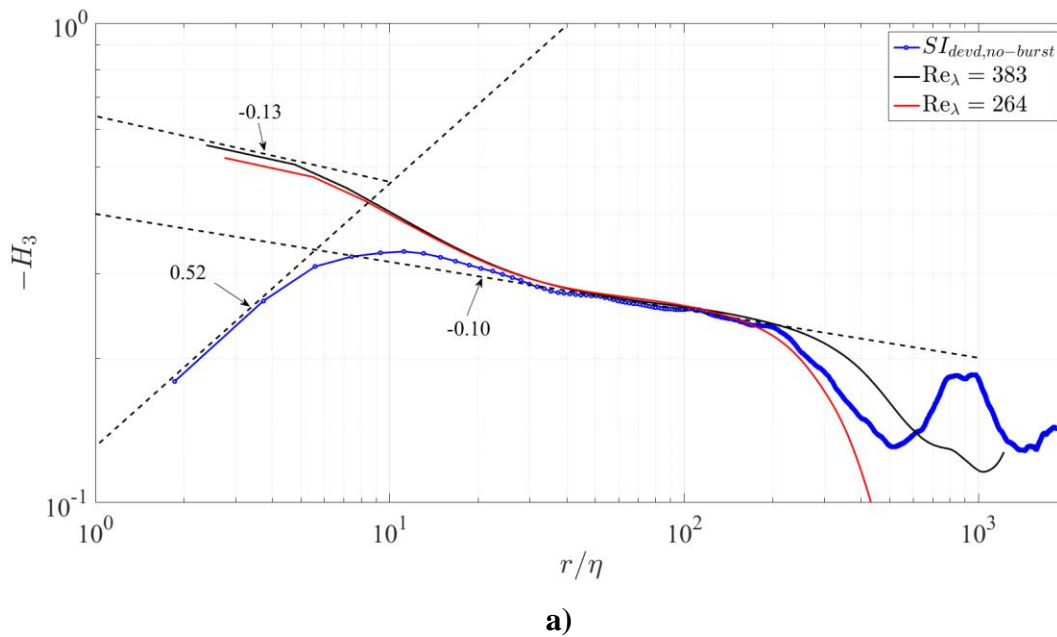
3.3 Comparisons of Various Structure Function Moments in Experiments and Simulations.

The results of Section 3.2 for odd moments led us to conduct a detailed comparison of normalized (canonical and modified) moments obtained via DNS and field experiments. We started with the third moment due to its relation to the corresponding structure function, for which classical theoretical results based on Kolmogorov equation [5] are available. All meaningful field results were obtained for the no-burst events. Events with burst did not provide sensible plots for interpretation.

In Figures 3 and 4, respectively, the results are presented for 3rd and 5th order canonical and modified structure functions; see eq. (1) and (2) for definitions. Obviously, the modified moments make sense only for odd moments. It is worth noting that canonical moments can be sensitive to intermittency, as it may affect differently the moments in the numerator and denominator, which are of different order. It is noted in [53] that odd moments of the same order $L_p(r)$ and $L_p^*(r)$ depend similarly on the intermittency and, therefore, normalization using $L_p^*(r)$ can significantly decrease the influence of intermittency on the scaling exponent.

Figure 3a indicates almost perfect agreement between the experimental and DNS canonical moments in the *inertial range*, which decay as $H_3=L_3/(L_2)^{3/2} \sim (r/\eta)^{-0.1}$. Since this appealing result was obtained in two physically different systems, at notably different characteristic Re_λ , it was necessary to analyze these outcomes with care to elicit the similarity of turbulence structures.

In the *viscous sub-range*, at small normalized separations $r/\eta < 10$, the results of Figure 3a show different behavior, and the scaling exponents are even of different sign for field and DNS data.



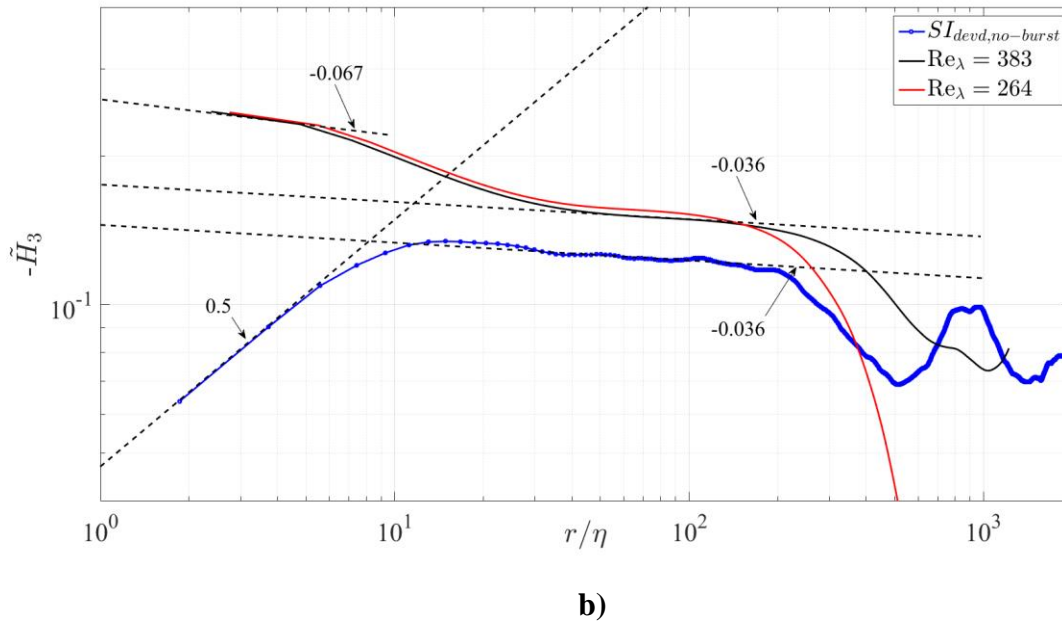


Figure 3. Comparison of the 3rd canonical (a) and modified (b) moments obtained in the field campaign [51, 52] with $Re_\lambda = 1200$ and DNS conducted for the 2 highest $Re_\lambda = 264$ and 383. The periods indicated in the legends are for time periods without bursts, determined according to the methodology of [52].

The DNS-Field \tilde{H}_3 comparisons shown in Figure 3b indicate that in the *inertial* sub-range the structure functions are *qualitatively* in very good agreement. The scaling exponents at the highest Re_λ , in spite of being very low (3.6%), are practically the same for DNS and field data. The *quantitative* agreement is less satisfactory compared to the canonical third moment. In contrary to scaling exponents in the *inertial* sub-range, Figure 3a shows that in the *viscous* sub-range the scaling exponents for the 3rd canonical moments are different for the field and DNS data. Similar trends are evident in Figure 3b, again indicating exponents of different signs for field and DNS data in the viscous sub-range.

Increasing the rank of the moments inevitably decreases the accuracy since the effect of greater velocity increments becomes more substantial and the resolution worsens due to their lower probability. Therefore, employing odd moments higher than the 5th seemed unreasonable. The canonical and modified 5th moments calculated for field and DNS data are presented in Figures 4a and 4b, respectively. In the *inertial* range, they are in almost perfect agreement with regard to slope

(-0.25) but not the amplitude. For example, in Figure 4a, at $r/\eta = 100$, the amplitude is 4.3 for field and 3 for DNS data. In the *viscous* sub-range ($r/\eta < 10$), however, the slope is negative (-0.35) in DNS (Figure 4a) and fluctuating in the field data; this contrasts field observations for the 3rd canonical moment, wherein a slope of about 0.5 was noted (Figure 3a).

In the *inertial* sub-range, for 5th order *modified* moments obtained using field and DNS data (Figure 4b), the slope is slightly positive (~1.5% for both). In the *viscous* sub-range, the slope is moderately negative (-9.5%) for DNS, but is fluctuating for field data as in the case of 5th *canonical* moments in Figure 4a.

Let us first consider *modified* structure functions of the odd 3rd and 5th order moments since their expressions include the moments of the same order in numerator and denominator. It has been widely assumed [11-14, 20-22] that 3rd order moments based on velocity increment and its modulus have very similar scaling in the *inertial* and *viscous* subranges, and in each the exponent differ only by a few percent. Our (nearly HIT) DNS data confirm this assumption, but field data (stratified turbulence in nocturnal boundary layer) show this trend only in the *inertial* sub-range; in the *viscous* sub-range, the scaling exponents differ substantially to the extent that even the sign of the slope can be different between DNS and field. Since the expectation for the *viscous* sub-range was a linear dependence of velocity increment on separation r , this result was highly unexpected. The results for the 5th order *modified* structure function in the *viscous* sub-range was even more puzzling since the moments were randomly fluctuating without a firm dependence on separation r .

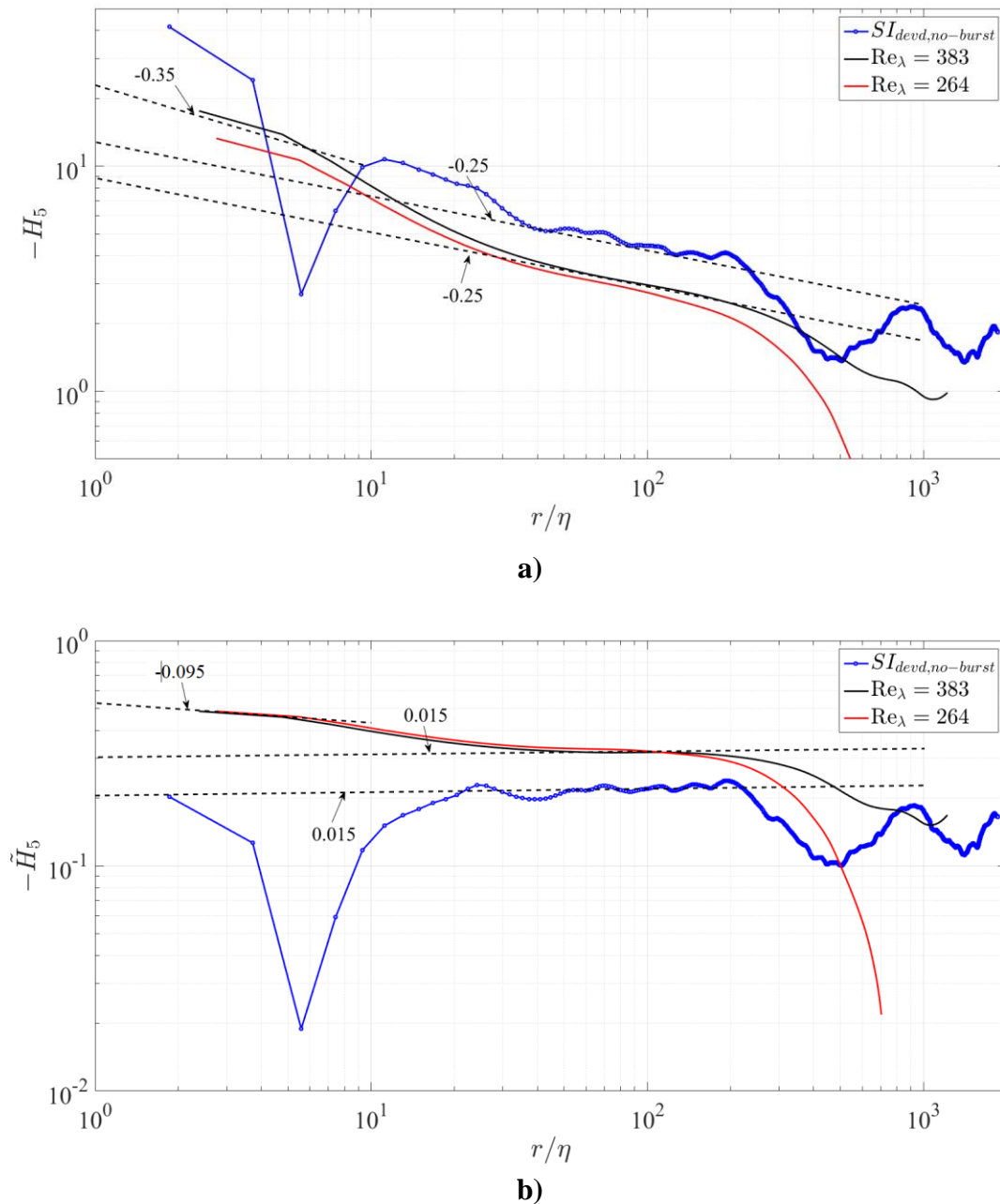


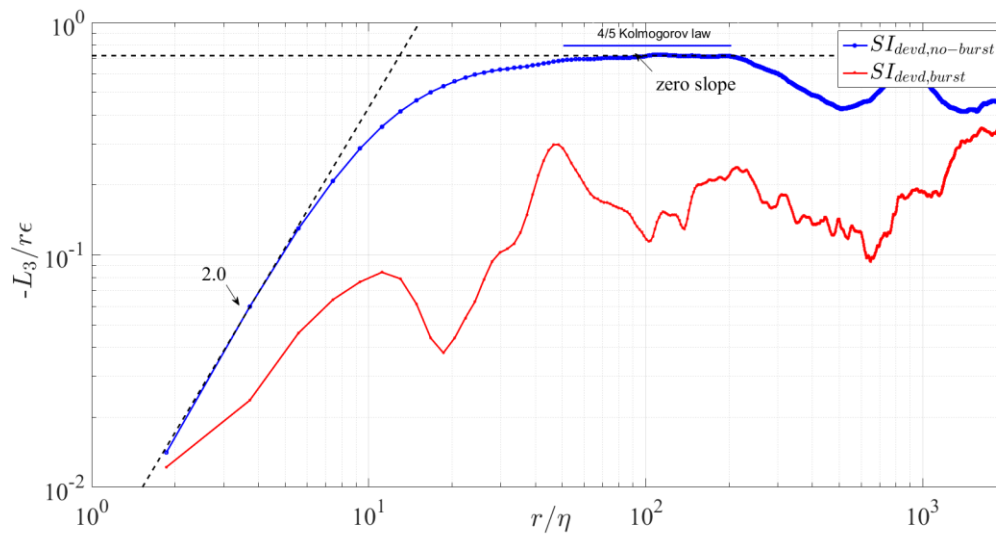
Figure 4. Comparison of 5th canonical moments (a) and modified moments (b) obtained in the field and DNS.

Unexpectedly, in the *viscous* sub-range, the *canonical* 3rd and 5th order moments (Figures 3a and 4a) normalized by the power $p/2$ of the second moment (that lineages to KSSH) behaved very similar to the *modified* moments of the same order (Figures 3b and 4b). In particular, the scaling exponents of the 3rd order moment were practically the same (0.50 for *modified* and 0.52 for *canonical* moments) and the 5th order *canonical* moment fluctuated randomly similarly to the case

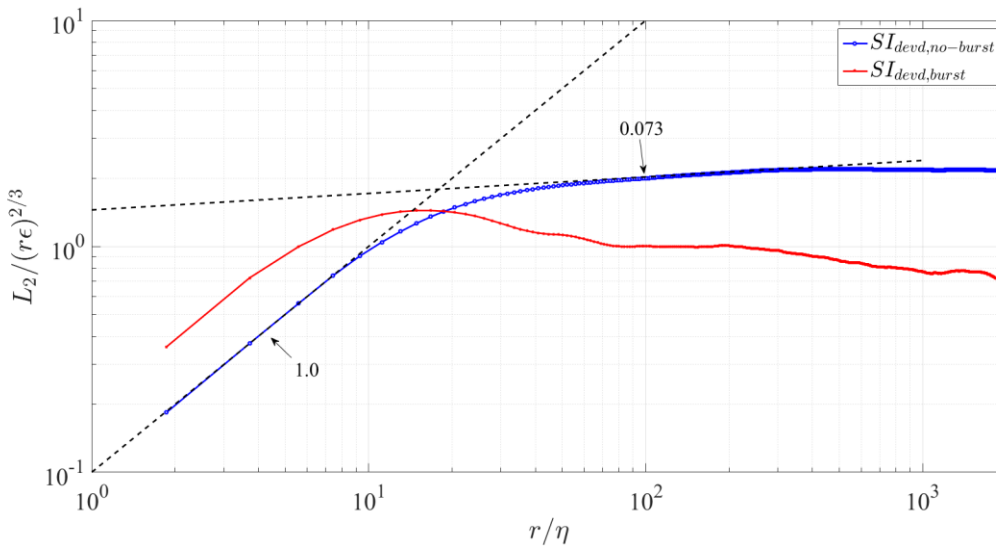
of the 5th order *modified* moment. Recall that the *modified* normalization was suggested in [53] to ameliorate intermittency effects by using moments of the same order in the numerator and denominator. Therefore, the expectation was that due to different normalization the *canonical* and *modified* moments will behave differently in the *viscous* sub-range. To clarify these findings, the structure functions $L_p(r)$ normalized using Kolmogorov *inertial* sub-range scaling $(r\varepsilon)^{p/3}$ were investigated.

The 2nd and 3rd order structure functions, which are directly related to turbulence dynamics and appearing in the Kolmogorov equation [K41, 1], are considered first. In Figure 5, the KSSH-normalized 3rd and 2nd order structure functions obtained in the field campaign are presented. As expected from the Kolmogorov equation, for the no-burst case, the normalized 3rd order longitudinal structure function approximately satisfied 4/5 law (Figure 5a), with an approximately zero slope in the *inertial* sub-range. In the *viscous* sub-range, the slope of the normalized 3rd longitudinal structure function is 2, or $L_3 \propto r^3$, indicating that $\Delta u(x, r) \propto r$. Figure 5b shows, however, for the same viscous subrange, $L_2 / (r\varepsilon)^{2/3} \propto r$ or $L_2 \propto r^{5/3}$, indicating that $\Delta u(x, r) \propto r^{5/6}$ and not the expected $\Delta u(x, r) \propto r$.

While above discussion concerned the *no-burst* case, it is noteworthy that in the *viscous* sub-range similar slopes were obtained for the 2nd order structure function for the case with *bursts* (Figure 5b). No clear scaling was observed in the *inertial* sub-range for datasets with bursts. For the 3rd order structure functions, no clear scaling was observed either in the *viscous* or *inertial* sub-ranges for the burst cases.



a)



b)

Figure 5. Normalized according to KSSH 3rd (a) and 2nd (b) order structure functions in field experiments computed using longitudinal velocity increment $\Delta u(x, r)$.

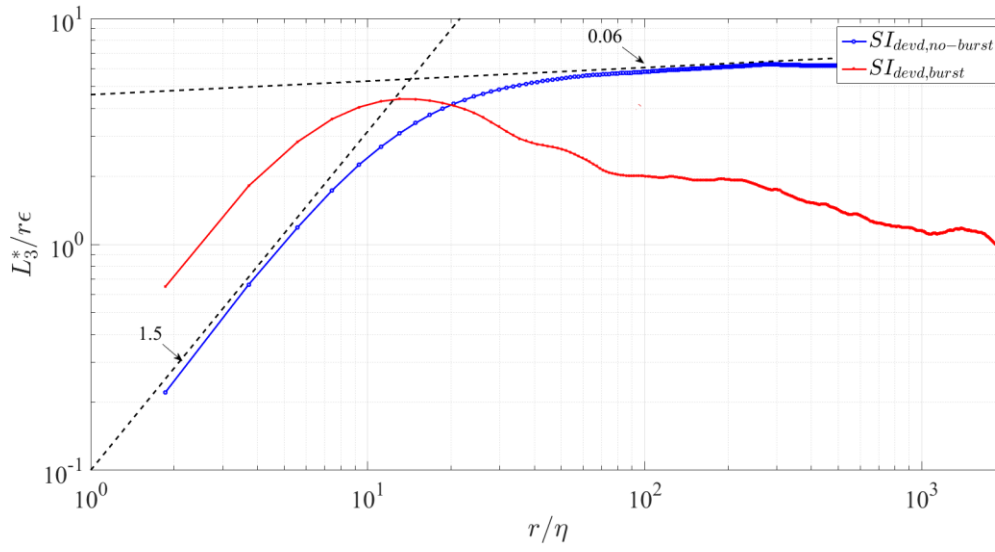
The near-zero negative (-0.13) slope of the canonical 3rd order structure in DNS (Figure 3a) attests to similar dependence of 2nd and 3rd structure functions on r/η in the *viscous* sub-range. Such behavior is expected, and has been observed in laboratory experiments with homogeneous flows (developed turbulence in a jet and past a cylinder) [13], however, in the field data (Figure 5) the

dependences of 2nd and 3rd structure functions on r/η differ in the *viscous* sub-range. This results in a slope of ~ 0.5 in the *viscous* sub-range for the 3rd order canonical structure function (Figure 3a).

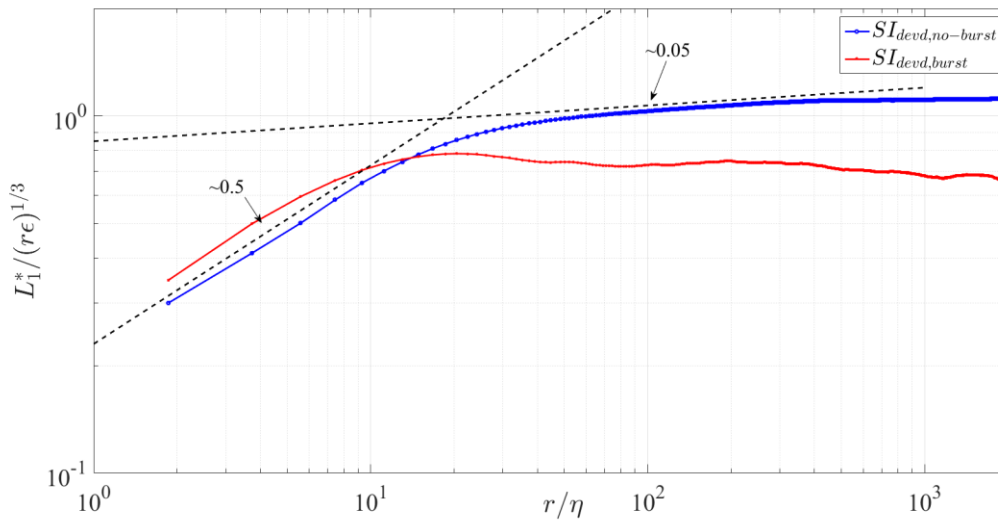
In the *inertial* sub-range, the slope of normalized 2nd order structure function is ~ 0.073 (Figure 5b), yielding a scaling exponent of 0.74 (i.e. $L_2(r) \propto r^{0.74}$) instead of 0.667 expected from KSSH, $L_p(r) \propto (r\varepsilon)^{p/3}$. This explains the slope -0.1 in Figure 3a of the 3rd canonical structure function. From eq. 2, it follows that $H_3(r) = L_3(r)/(L_2(r))^{3/2} \propto r^{-0.11}$ (i.e. the exponent yielding $1 - 0.74 \cdot 1.5 = -0.11$, which is very close to -0.1). Similar results are found in the literature [11, 12].

The above observations prompted investigations into all other (viable) even and odd structure functions for $\Delta u(x, r)$ and $|\Delta u(x, r)|$. Note that even moments are identical for both types of velocity increments. In the following, additional results are presented for the 3rd and 1st order structure functions for modulus $|\Delta u(x, r)|$ (Figure 6) and 4th and 6th (Figure 7) order structure functions. The 1st order structure function for $\Delta u(x, r)$ is identically zero. The 3rd order structure function for $\Delta u(x, r)$ was presented in Figure 4a.

It follows from Figure 6 that the shapes in the *viscous* sub-range ($r/\eta < 10$) are $L_1^* \propto r^{5/6}$ for the 1st order and $L_3^* \propto r^{15/6}$ for the 3rd order structure functions, suggesting $|\Delta u(x, r)| \sim r^{5/6}$ as observed with 2nd order structure functions (Figure 5b) and not to the separation r as observed with the 3rd order structure function for $\Delta u(x, r)$. In the *inertial* sub-range, structure functions for both $|\Delta u(x, r)|$ and $\Delta u(x, r)$ almost follow Kolmogorov scaling, although a slight deviation was evident. As established earlier, in the *viscous* sub-range, both 3rd and 1st order structure functions evaluated for $|\Delta u(x, r)|$ with all datasets, including those with bursting events, has the same scaling (Figure 6a and b). In the *inertial* sub-range, when bursting is present, the structure function is randomly varying and no definite scaling is observed.



a)

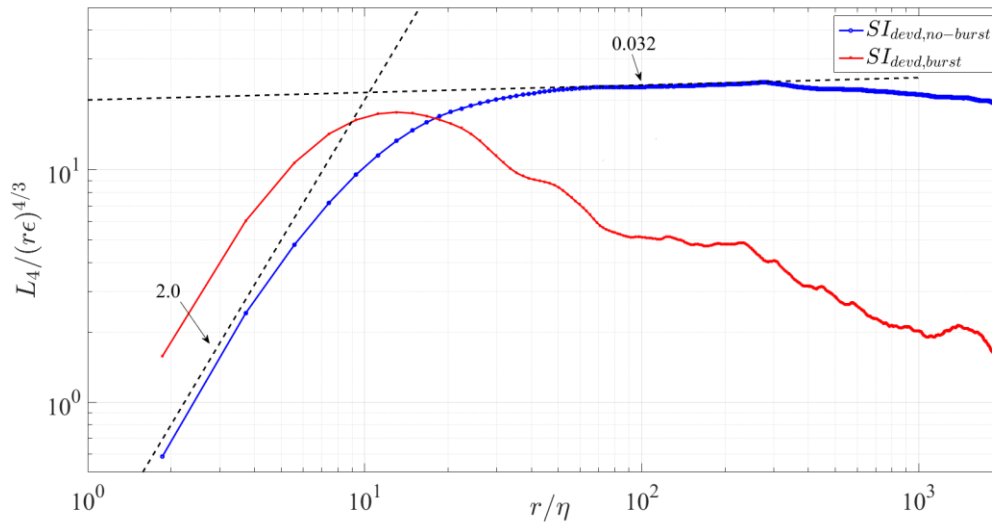


b)

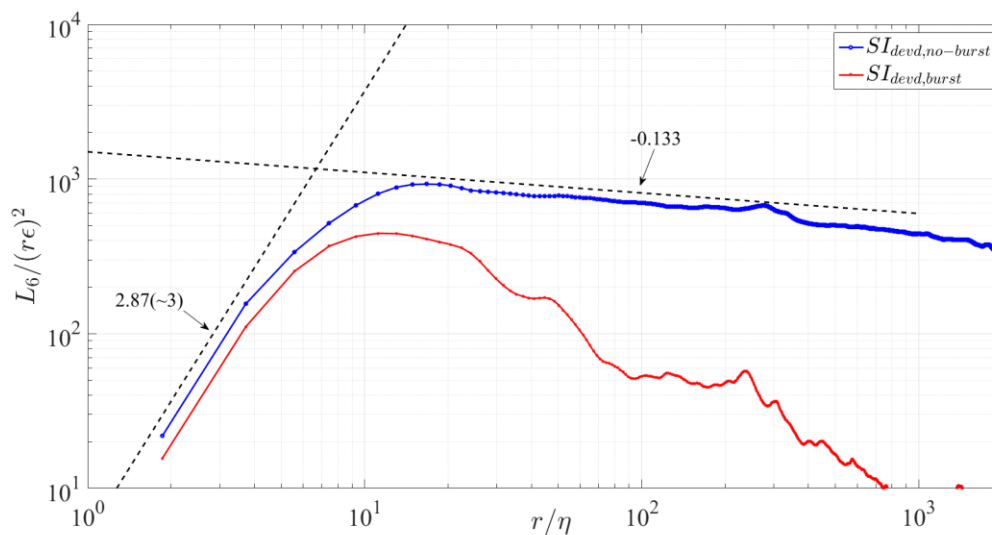
Figure 6. Normalized odd 3rd (a) and 1st (b) order structure functions in field experiments computed using modulus of velocity increment.

The 4th and 6th order canonical structure functions in Figure 7 confirm the same trend as observed above for 1st, 2nd, and 3rd structure functions for $|\Delta u(x, r)|$. In the *viscous* sub-range, the velocity increment $|\Delta u(x, r)|$ is found to be proportional to $r^{5/6}$ for both datasets with and without bursts. This power-law is also clearly confirmed for the 4th order and is nearly valid for the 6th order

structure function. In the *inertial* sub-range, the 4th order structure function approximately adheres to Kolmogorov scaling, and an anomaly becomes noticeable only when the 6th order structure function is considered.



a)



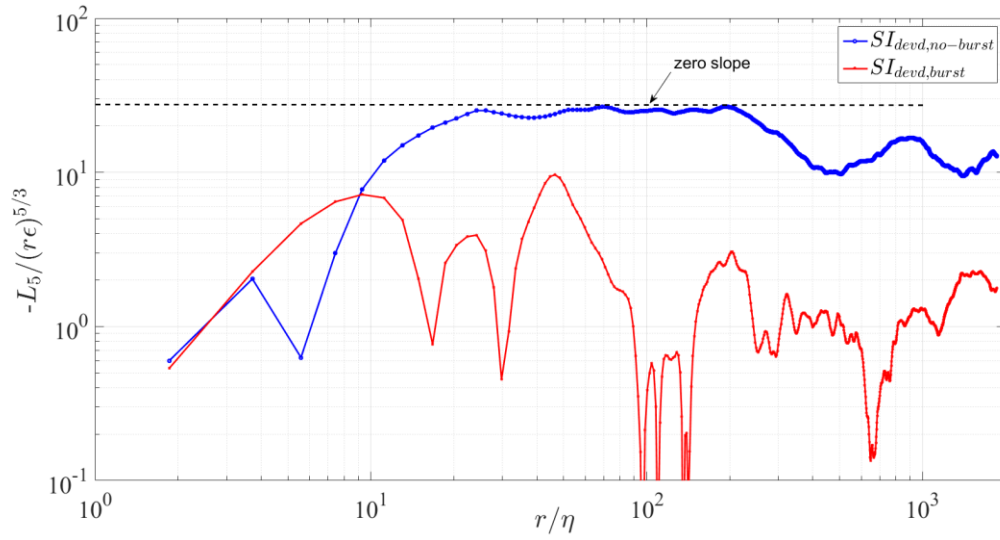
b)

Figure 7. Normalized according to KSSH even 4th (a) and 6th (b) order structure functions in field experiments computed using longitudinal velocity increment.

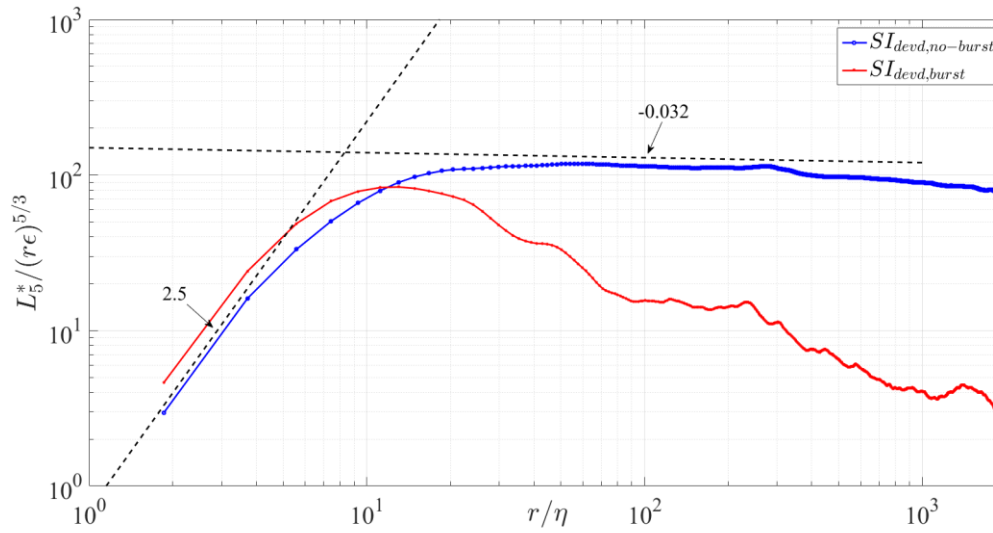
In particular, the slope of 4th order structure function in the inertial sub-range is very small (Figure 7a), about 3%, but unexpectedly positive, marginally exceeding KSSH prediction. The slope of the 6th order structure function (Figure 7b) in the same inertial sub-range is negative, thus confirming the well-known anomaly [13-17] that scaling exponent is lower than $p/3$ for high order structure functions, which for our field experiments $p \geq 5$. The deviations from Kolmogorov scaling exponent noted in the literature [13-17] either obtained in the laboratory or DNS, however, is notably greater than that evaluated from our field data.

The normalized 5th order structure functions based on KSSH for $\Delta u(x, r)$ and $|\Delta u(x, r)|$ were calculated and are presented in Figures 8a and 8b. In the *inertial* sub-range (around $r/\eta = 100$) the normalized 5th order structure function (Figure 8a) is undulating about KSSH-predicted zero slope, however in the *viscous* sub-range the structure function fluctuates randomly without a clear trend. No linear dependence between velocity increment $\Delta u(x, r)$ and separation r exists for the 5th order structure function on the contrary to that observed for the 3rd order structure function (Figure 5a).

The 5th order normalized structure function for $|\Delta u(x, r)|$ behaves essentially different (Figure 8b) from its $\Delta u(x, r)$ counterpart, with very smooth curves both in the *inertial* (around $r/\eta = 100$) and *viscous* sub-ranges. The slope in the *inertial* sub-range is approximately zero for the no-burst case, but a slight negative slope ($\approx -3\%$) is evident. The shape of this structure function in the *viscous* sub-range ($r/\eta < 10$) is about $L_\zeta^* \propto r^{25/6}$, corresponding to $|\Delta u(x, r)| \propto r^{5/6}$, same as that observed for odd 1st and 3rd order structure functions (Figures 6a and 6b) and for all even structure function studied here (2, 4 and 6). The same slope of 25/6 was observed in the *viscous* sub-range for both burst and no-burst cases. In the *inertial* range, no clear scaling was observed with bursts.



a)



b)

Figure 8. Normalized 5th order structure functions in field experiments computed using longitudinal velocity increment $\Delta u(x, r)$ (a) and its modulus (b).

The scaling exponents in the *inertial* and *viscous* sub-range structure functions of different orders varying from 1st to 6th are summarized in Figure 9. Although our field results in the *inertial* sub-range do not contradict with those previously reported for HIT [11, 19-23], there are modest qualitative discrepancies. The significant differences are in the small values of separation r/η in the

viscous sub-range. A widely-used assumption is that in the *viscous* sub-range (which have received lesser attention in the past) both $\Delta u(x, r)$ and $|\Delta u(x, r)|$ vary similarly and nearly linear with r [13, 14]. This assumption is of practical interest for Extended Self Similarity (ESS), which suggests replacing \mathcal{E} of Kolmogorov normalization with 3rd order structure function for $|\Delta u(x, r)|$.

According to our field results, for the 3rd order structure functions in the *viscous* sub-range behave as $\Delta u(x, r) \propto r$ and $|\Delta u(x, r)| \propto r^{5/6}$, revealing appreciably different behavior between the two. Only the last relation, $|\Delta u(x, r)| \propto r^{5/6}$, is confirmed for the 5th order modulus structure function (Figure 8b); instead of linear dependence with r , the 5th order conventional structure function for $\Delta u(x, r)$ (Figure 8a) fluctuates randomly in the *viscous* sub-range.

A surprising result is that in the *viscous* sub-range *all* structure functions of the *modulus* of the velocity increment in our study are described by the unique equation $\langle |\Delta u(x, r)|^p \rangle \propto r^{5p/6}$ for $p \in (1 - 6)$ (Figure 9). The odd structure functions ($p = 1, 3, 5$) are definitely different for $\Delta u(x, r)$ than for $|\Delta u(x, r)|$. In particular, the 1st order structure function for $\Delta u(x, r)$ is identically zero. The 5th order structure function (Figure 8a) in the *viscous* sub-range did not allow determining the scaling exponent unambiguously. One could expect it to behave similarly to the 3rd order structure function (i.e., vary linearly with r). However, in our field experiments, disparities exist between 3rd and 5th order structure functions, and it is highly probable that they are due to stable-stratification effects of the nocturnal ABL, as discussed below.

In our DNS of HIT, all scaling exponents of odd structure functions ($p = 3, 5, 7$) are approximately the same (Figure 2) for $\Delta u(x, r)$ and $|\Delta u(x, r)|$. Additionally, in contrary to field results (Figure 4a), the shape of the 5th order structure function for $\Delta u(x, r)$ is smooth. Interestingly, in the *viscous* sub-range calculations with field data, similar scaling exponents are also obtained for all structure functions for $|\Delta u(x, r)|$, including for data containing bursts. Conversely, for datasets with bursts, no definite scaling exponents are obtained in the *inertial* sub-

range with any type of velocity increment, including $|\Delta u(x, r)|$. This indicates that bursts mostly affect scales larger than those of viscous sub-range.

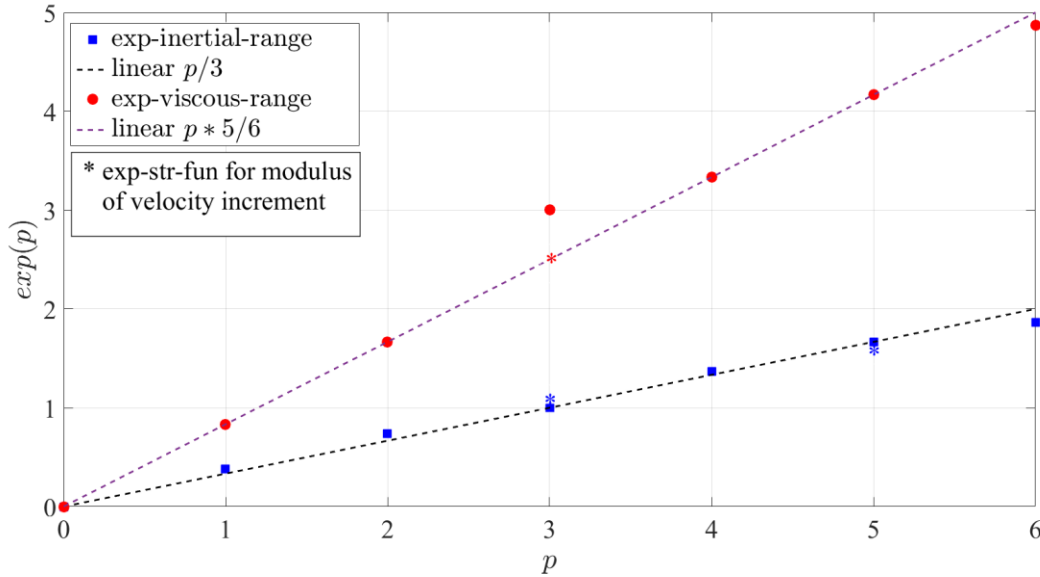


Figure 9. Scaling exponents of the structure functions in the *inertial* and *viscous* sub-ranges for velocity increment and its modulus evaluated for field data. Stars indicate that different scaling exponents of structure functions (exp-str-fun) were obtained with odd 3rd and 5th structure functions for velocity increments and their modulus.

The results for scaling exponents obtained in the present case of stratified ABL (dubbed *str*) are presented in Table 1 along with their HIT counterparts (dubbed *hom*), with strong shear near the boundary (*sh*), theoretical predictions in accordance to KSSH (*kssh*) in the inertial sub-range and linear dependence on r (*lin*) in the viscous sub-range. As mentioned, it is commonly accepted that scaling exponents for velocity increment and its modulus are practically the same across all sub-ranges, and this claim has been partially verified in studies dealing with ESS of HIT [11, 13]. Our results cast doubts on the *general* validity of this statement and, therefore, detailed results were presented for structure functions based on $\Delta u(x, r)$ and $|\Delta u(x, r)|$ for *inertial* and *viscous* sub-ranges.

Naturally, only odd structure functions are relevant, since even functions are identical for $\Delta u(x, r)$ and $|\Delta u(x, r)|$ cases. The small differences between scaling exponents of 3rd and 5th order structure functions in the *inertial* sub-range are within the uncertainty of the analysis, but in the *viscous* sub-range the differences are substantial (Table 1). In the *inertial* sub-range, scaling exponents of the 4th, 5th and 6th order structure functions are considerably closer to Kolmogorov scaling (than their counterparts in flows with strong shear). The scaling exponent of the 2nd order structure functions, however, shows greater deviation from Kolmogorov scaling, thus contradicting the assumption of possible decrease of intermittency due to stable stratification.

The assumption of increased intermittency in *strong shear flow* seems plausible since the scaling exponents of all orders (1st, 2nd, 4th, 5th, 6th) in the *inertial* sub-range show an increased deviation from KSSH-based scaling exponent obtained in HIT simulations/experiments. The exponent of 3rd order structure function is 1 in *all* cases, in agreement with the Kolmogorov equation. In the *viscous* sub-range, direct results for scaling exponents are not reported in published papers, but indirect results, including our DNS, where canonical and modified moments were calculated, show that the exponents for $\Delta u(x, r)$ and $|\Delta u(x, r)|$ for HIT are nearly the same.

The situation is different for stratified nocturnal ABL turbulence. The 3rd structure function for velocity increment in the *viscous* sub-range shows predicted linear dependence, but the 5th order structure function shows strong fluctuations thus precluding the determination of a scaling exponent. *All* structure functions for *modulus* of velocity increment, except the 6th order where a slight deviation was present, are yielding the scaling exponent $5p/6$.

Table 1 Scaling exponents of the (structure) functions in the inertial and viscous sub-ranges for velocity increment and its modulus for datasets without bursts. *kssh* and *lin* - theoretical exponents in *inertial* - $p/3$ and linear - p in *viscous* sub-ranges [18], *hom* and *sh* – experimental and DNS values in HIT and shear flows [28], *str* –current field data measured under stratified conditions in nocturnal ABL. In viscous sub-range results for modulus of velocity increment corresponding to $5p/6$.

structure functions of order p	$\Delta u(x, r)$ scaling exponents inertial sub-range <i>kssh, hom, str, sh</i>	$ \Delta u(x, r) $ scaling exponents inertial sub-range <i>kssh, hom, str, sh</i>	$\Delta u(x, r)$ scaling exponents viscous sub-range <i>lin, hom, str, sh</i>	$ \Delta u(x, r) $ scaling exponents viscous sub-range <i>lin, hom, str, sh</i>
1	Function identically 0	0.333, 0.36, 0.38 , 0.44	Function identically 0	1.0, n/a*, 0.833 , n/a
2	0.667, 0.70, 0.74 , 0.77		2.0, n/a, 1.667 , n/a	
3	1.0, 1.0, 1.0 , 1.0	1.0, n/a, 1.06 , n/a	3.0, n/a, 3.0 , n/a	3.0, n/a, 2.50 , n/a
4	1.333, 1.28, 1.334 , 1.17		4.0, n/a, 3.333 , n/a	
5	1.667, n/a, 1.667 , n/a	1.667, 1.54, 1.635 , 1.31	5.0, n/a, fluct , n/a	5.0, n/a, 4.1667 , n/a
6	2.0, 1.78, 1.867 , 1.44		6.0, n/a, 4.87 , n/a	

*n/a – not available from experiments or DNS

The above results call for a plausible physical explanation. Note that the flow arriving at the ES-2 tower (equipped with the combo-probe [52]) originated at the Granite Mountain slope [51, 52] as a nocturnal katabatic flow. As it drains under stably stratified condition, turbulence generated within is also advected and evolved, possibly becoming nearly HIT at ES2 [52, 56], much the same way as in wind-tunnel stratified flows [46]. When stratification is very weak, the turbulence remains HIT type, but when stratification becomes stronger, turbulence is buoyancy dominated, causing PDF to be almost symmetrical. Our initial attempts to *qualitatively* assess the effect of moderate stratification on structure functions based on previous laboratory results by blending fluctuations from isotropic and anisotropic sectors at fine scales appear to explain the linear dependence between velocity increment and separation for the 3rd order normalized structure function (according to KSSH) in the *viscous* sub-range and why such dependence does not hold for the 5th order normalized structure function. Such decomposition also allows obtaining different behavior for structure functions constructed for the absolute velocity increment $|\Delta u(x, r)|$. Presentation of this assessment is left for a future publication.

When laboratory grid generated HIT [46] is subjected to thermally generated stable stratification, turbulence becomes *anisotropic*, and the relevant controlling parameter of overall flow is the inverse of internal/turbulent Froude numbers, $Fr = \varepsilon / Nu'^2$ where u' is the RMS of velocity component, N the buoyancy frequency and ε the rate of dissipation. The typical inverse Froude numbers assessed in our field experiments were $2 \div 5$ [56], coincidentally in the same range as that observed in laboratory flows of [46], thus providing peripheral support for the notion of anisotropic turbulence at ES-2. Also note that the controlled laboratory results of [46] were obtained at relatively low $Re_\lambda \sim 20-40$ and that Fr does not specifically address the nuances of stratification-effects, such as their penetration to viscous scales. As such, the observed in the field peculiar behavior of third *canonical* and *modified* structure functions and their departure from the HIT data results following from DNS needs further investigation.

A rigorous attempt to separate isotropic and anisotropic contributions can be made in the framework of $SO(3)$ formalism by conducting the decomposition of appropriately measured structure or correlation functions into spherical harmonics [44, 45, 57]. However, this requires simultaneous multi-points measurement of high-frequency oscillating velocities and velocity derivatives and is left for future work.

4. Summary

1. The nocturnal stable boundary layer data acquired during the MATERHORN field program [51] were separated into “no-bursts” and “bursts” periods as in [52]. The no-burst field dataset as well as DNS datasets of homogeneous isotropic turbulence (HIT) were used to study the structure functions of various order of the velocity increment $\Delta u(x, r)$ and its modulus $|\Delta u(x, r)|$.
2. The canonical structure function is obtained by normalizing higher order structure functions of order p by the 2nd order structure function in power $p/2$ (eq. 2). When structure functions of different orders are involved, this normalization can result in significant variation of the scaling exponent, for example, due to different anomalies caused by intermittency. Such effects are

expected to magnify if the contributions from anisotropic sectors are accounted [38, 41], as in the case of shear and/or stratification. The computation of odd higher order structure functions (third, fifth and seventh) for $\Delta u(x, r)$ using four DNS datasets of HIT showed that although scaling exponents do not depend substantially on Re_λ , the data are not collapsing in the inertial and viscous sub-ranges, indicating that scaling used is unsatisfactory.

3. A new (modified) normalization proposed for skewness of longitudinal velocity derivative $\partial u / \partial x$ by [53] involves the replacement of the second moment in the denominator of the canonical scaling with the same order 3rd moment of the modulus $|\partial u / \partial x|$. This new scaling was adopted for odd higher order structure functions (third, fifth and seventh) of $\Delta u(x, r)$, which were computed using DNS datasets of HIT. The results were striking: for all moments, a conspicuous collapse was achieved in the viscous and inertial sub-ranges at all Re_λ used in the study, suggesting the efficacy of new scaling for all moments. The collapse does not occur at larger scales, which is due to computational box boundaries and turbulence forcing at larger scales.
4. Detailed comparison of odd 3rd and 5th order canonical and modified moments evaluated using field data without bursts with their DNS counterparts indicated a very good agreement in the inertial sub-range $50 \leq r / \eta \leq 200$; for example, at $r / \eta = 100$, both field and DNS simulations at the highest Re_λ yield the same scaling exponents. In the viscous sub-range, the 3rd canonical and modified structure functions at small separations varies with separation as $\sim (r / \eta)^{0.5}$ in contrast to the approximately constant value exhibited by DNS.
5. The structure functions (of order p) in the nocturnal ABL is normalized according to Kolmogorov Self Similarity Hypothesis (KSSH) as $L_p(r) / (\epsilon r)^{p/3}$; and for the 3rd moment it yielded the predicted linear dependence $\langle \Delta u(x, r)^3 \rangle \propto r^3$ for smaller separations in the *viscous* sub-range. On the contrary, the 2nd moment in the *viscous* sub-range does not support the predicted r^2 dependence, but yielded $\langle \Delta u(x, r)^2 \rangle \propto r^{5/3}$. This explains the surprising scaling exponent of ~ 0.5 for canonical 3rd order structure function in the *viscous* sub-range.
6. Since even moments are identical for velocity increment and its modulus, in the *viscous* sub-range the r dependence for the 2nd moment could be extended for a general p -order moment

as $\langle |\Delta u(x, r)|^p \rangle \propto r^{5p/6}$, which was (at least approximately) supported by our field data for all p ($1 \div 6$) used.

7. As implied from item (5) above, in the *viscous* sub-range of the stratified turbulence measured in the field the 3rd order structure functions of the velocity increment $\Delta u(x, r)$ and its modulus $|\Delta u(x, r)|$, normalized according to KSSH, behave differently. The same data processing approximately confirmed 4/5 Kolmogorov law for the *inertial* sub-range. The canonical and modified 3rd order structure functions computed for the same data showed very good agreement with their counterparts obtained in DNS for the *inertial* sub-range, however, a substantial disparity was observed in the *viscous* sub-range.
8. In the *viscous* sub-range of DNS, the scaling exponent of the modified 3rd order structure function is close to zero, indicating that, in contrast to field observations, the scaling exponents for velocity increment $\Delta u(x, r)$ and for its modulus $|\Delta u(x, r)|$ for HIT are nearly the same.
9. As in the case of 3rd order, the canonical and modified 5th order structure functions computed using field data showed very good agreement with their DNS counterparts for the *inertial* sub-range. In the *viscous* sub-range, both the canonical and modified 5th order structure functions for field data were oscillating, and the scaling exponents could not be determined.
10. The field data set represents stratification-affected high Reynolds number turbulence in a katabatic flow in the nocturnal ABL [56]. An attempt was made to isolate stratification effects from the total turbulence field using a simple-minded assumption that the measured turbulence at 6 m above the ground is contributed by two uncorrelated effects: roughly HIT generated within the katabatic flow arriving from a nearby Granite mountain and motions due to stable temperature stratification at the measurement location (i.e., ES-2 tower). In ABL, shear effects are substantial near the ground, however, at larger distances (e.g., 6 m height) turbulence tends toward HIT which can be affected by anisotropic tendency of stratification [46, 47] that may even penetrate to fine scales. A simplified model based on blending of fluctuation contributions from isotropic and anisotropic sectors at fine scales appear to explain the linear dependence between velocity increment and separation for the 3rd order normalized structure function in the *viscous* sub-range and why such dependence does not hold for the 5th order normalized structure function (which is deferred to a future publication). In addition, such decomposition allows obtaining of different behavior for structure functions constructed for

the absolute velocity increment $|\Delta u(x, r)|$. Considering all, we suggest that the more sophisticated $SO(3)$ formalism [57] developed for decomposition of structure and/or correlation functions to separate contributions of isotropic and anisotropic sectors be attempted in future studies of anisotropy at small scales introduced by large scale effects such as stratification. Studies on small and viscous scales have become one of our foci because of the interest in understanding fog formation mechanisms, where spawning of water droplets occurs at Kolmogorov and sub-Kolmogorov scales of ABL. We hope that this work provides entrée for future such work.

Acknowledgement: This research was funded by the Israel Science Foundation (Grant 408/15, EK), US Office of Naval Research Grant N00014-21-1-2296 (Fatima MURI, HJSF/EK) and US National Foundation Grant AGS-1921554 (HJSF).

References

1. Kolmogorov, A.N. The local structure of turbulence in incompressible viscous fluid for very large Reynolds numbers, *Dokl. Akad. Nauk SSSR*. **30**, 301-305 (1941).
2. Batchelor, G.K. and Townsend, A.A. The nature of turbulent motion at large wave-numbers. *Proc. R. Soc. London A* **199**, 238-255 (1949).
3. Kuo, A.Y.S. and Corrsin, S. Experiments on internal intermittency and fine-structure distribution functions in fully turbulent fluid. *J. Fluid Mech.* **50**, 285-320 (1971).
4. Rose, H.A. and Sulem, P.L. Fully developed turbulence and statistical mechanics. *Journal de Physique* **39(5)**, 411-484 (1978).
5. Frisch, U. *Turbulence: The legacy of A.N. Kolmogorov* (Cambridge University Press, Cambridge, 1995).
6. Pouquet, A. Intermittent Turbulence in a Global Ocean Model. *Physics* **11**, 21 (2018).
7. Rorai, C.; Mininni, P.D. and Pouquet, A. Turbulence comes in bursts in stably stratified flows. *Phys. Rev. E* **89**, 043002 (2014).
8. Feraco, F.; Marino, R.; Pumir, A.; Primavera, L.; Mininni, P. D.; Pouquet, A. and Rosenberg, D. Vertical drafts and mixing in stratified turbulence: Sharp transition with Froude number. *EPL* **123**, 44002 (2018).
9. Ishihara, T.; Gotoh, T. and Kaneda, Y. Study of high-Reynolds number isotropic turbulence by direct numerical simulation. *Annu. Rev. Fluid Mech.* **41**, 165-80 (2009).
10. Ishihara, T.; Morishita, K.; Yokokawa, M.; Uno, A. and Kaneda, Y. Energy spectrum in high-resolution direct numerical simulations of turbulence. *Phys. Rev. Fluids* **1**, 082403(r) (2016).

11. Gotoh, T., Fukayama, D., and Nakano, T. Velocity field statistics in homogeneous steady turbulence obtained using a high-resolution direct numerical simulation. *Phys. Fluids* **14**(3), 1065-1081 (2002).
12. R. Benzi, S. Ciliberto, R. Tripiccone, C. Baudet, F. Massaioli and S. Succi Extended self-similarity in turbulent flows, *Phys. Rev. E* **48**, R29-R32 (1993).
13. R. Benzi, S. Ciliberto, C. Baudet, G. Ruiz Chavarria and R. Tripiccone Extended Self-Similarity in the Dissipation Range of Fully Developed Turbulence, *EPL* **24**, 275-279 (1993).
14. Briscolini, M., Santangelo, P., Succi, S. and Benzi, R. Extended self-similarity in the numerical simulation of three-dimensional homogeneous flows. *Phys. Rev. E* **50**, R1745-1747 (1994).
15. Benzi, R., Ciliberto, S., Baudet, C. and Ruiz Chavarria, G. On the scaling of three dimensional homogeneous and isotropic turbulence. *Physica D* **80**, 385–398 (1995).
16. Benzi, R., Biferale, L., Ciliberto, S., Struglia, M. V. and Tripiccone, R. Generalized scaling in fully developed turbulence. *Physica D* **96**, 162–181 (1996).
17. Anselmet, F., Gagne, Y., Hopfinger, E.J., and Antonia, R.A. High-order velocity structure functions in turbulent shear flows. *J. Fluid Mech.* **140**, 63-89 (1984).
18. M. Nelkin What do we know about self-similarity in fluid turbulence? *J. Stat. Phys.* **54**, 1-15 (1989).
19. She, Z.S., and Leveque, E. Universal scaling law in fully developed turbulence. *Phys. Rev. Lett.* **72**, 336-339 (1994).
20. Arneodo, A., Baudet, C., Belin, F., Benzi, R., Castaing, B., Chabaud, B., Chavarria, R., Ciliberto, S., Camussi, R., Chillia, F., Dubrulle, B., Gagne, Y., Hebral, B., Herweijer, J., Marchand, M., Maurer, J., Muzy, J. F., Naert, A., Noullez, A., Peinke, J., Roux, F., Tabeling, P., van de Water, W., Willaime H. Structure functions in turbulence, in various flow configurations, at Reynolds number between 30 and 5000, using extended self-similarity. *EPL*, **34**, 411-416 (1996).
21. Boratav, N., and Pelz, R. B. Structures and structure functions in the inertial range of turbulence, *Phys. Fluids* **9**, 1400-1415.
22. Grossmann, S., Lohse, D., and Reeh, A. (1997) Application of extended self-similarity in turbulence. *Phys. Rev. E* **56**, 5, 5473-5478 (1997).
23. Belin, F.; Maurer, J.; Tabeling, P. and Willaime, H. Velocity gradient distributions in fully developed turbulence, *Phys. Fluids*, **9**, 3843 – 3850 (1997).
24. Sreenivasan, K. R., and Dhruva, B. Is there scaling in high-Reynolds number turbulence? *Prog. Theor. Phys. Suppl.* **130**, 103-120 (1998).
25. Garg S., and Warhaft, Z. On small scale structure of simple shear flow. *Phys. Fluids* **10**, 662-673 (1998).
26. Shen X. and Warhaft, Z. The anisotropy of the small scale structure in high Reynolds number ($R_\lambda \sim 1000$) turbulent shear flow. *Phys. Fluids* **12**, 2976-2989 (2000).
27. Shen X. and Warhaft, Z. Longitudinal and transverse structure functions in sheared and unshered wind-tunnel turbulence. *Phys. Fluids* **14**, 370-381 (2002).

28. Toschi, F., Amati, G., Succi, S., Benzi, R. and Piva, R. Intermittency and Structure Functions in Channel Flow Turbulence. *Phys. Rev. Lett.* **82**, 5044-5047 (1999).
29. Benzi, R., Amati, G., Casciola, C. M., Toschi, F. and Piva, R. Intermittency and scaling laws for wall bounded turbulence. *Phys. Fluids* **11**, 1284-1286 (1999).
30. Toschi, F., Leveque, F. and Ruiz-Chavarria, G. Shear effects in nonhomogeneous turbulence. *Phys. Rev. Lett.* **85**, 1436 (2000).
31. Gualtieri, P., Casciola, C. M., Benzi, R., Amati, G. and Piva, R. Scaling laws and intermittency in homogeneous shear flow. *Phys. Fluids* **14**, 583-596 (2002).
32. Casciola, C. M., Benzi, R., Gualtieri, P., Jacob, B. and Piva, R. Double scaling and intermittency in shear dominated flows. *Phys. Rev. E* **65**, 015301 (2002).
33. Jacob, B., Olivieri, A. and Casciola, C. Experimental assessment of a new form of scaling law for near-wall turbulence. *Phys. Fluids* **14**, 481-491 (2002).
34. Casciola, C. M., Benzi, R., Gualtieri, P., Jacob, B. and Piva, R. Scale-by-scale budget and similarity laws for shear turbulence. *J. Fluid Mech.* **476**, 105-114 (2003).
35. Jacob B., Biferale L., Iuso G. and Casciola C.M. Anisotropic fluctuations in turbulent shear flows. *Phys. Fluids* **16**, 4135-4142 (2004).
36. Casciola, C. M., Gualtieri, P., Jacob, B. and Piva, R. Scaling properties in the production range of shear dominated flows. *Phys. Rev. Lett.* **95**, 024503 (2005).
37. Casciola, C. M., Gualtieri, P., Jacob, B. and Piva, R. The residual anisotropy at small scales in high shear turbulence. *Phys. Fluids* **19**, 101704 (2007).
38. Biferale, L., and Vergassola, M. Isotropy vs anisotropy in small-scale turbulence. *Phys. of Fluids* **13**, 2139 (2001). <https://doi.org/10.1063/1.1381019>.
39. Biferale, L. and Toschi, F. Anisotropic homogeneous turbulence: Hierarchy and intermittency of scaling exponents in the anisotropic sectors. *Phys. Rev. Lett.* **86**, 4831 (2001).
40. Biferale, L., Boffetta, G., Celani, A., Lanotte, A., Toschi, F. and Vergassola, M. The decay of homogeneous anisotropic turbulence. *Phys. Fluids* **15**, 2105-2112 (2003).
41. Arad, I., Dhruva, B., Kurien, S., L'vov, V.S., Procaccia, I. and Sreenivasan, K.R. Extraction of Anisotropic Contributions in Turbulent Flows. *Phys. Rev. Lett.* **81**, 5330-5333 (1998).
42. Arad, I., L'vov, V.S., and Procaccia, I. Correlation functions in isotropic and anisotropic turbulence: The role of the symmetry group. *Phys. Rev. E* **59**, 6753-6765 (1999).
43. Belinicher, V. I. and L'vov, V. S. A scale-invariant theory of fully developed hydrodynamic turbulence *Sov. Phys. JETP* **66** (2), 303-313(1988). (Translation from *Zh. Eksp. Teor. Fiz.* 93, 533-551 (August 1987)).
44. L'vov, V. S., Procaccia, I. and Tiberkevich, V. Scaling exponents in anisotropic hydrodynamic turbulence. *Phys. Rev. E* **67**, 026312 (2003).
45. Biferale, L. and Procaccia, I. Anisotropy in turbulent flows and in turbulent transport, *Phys. Rep.* **414** (2-4), 43-164 (2005). <https://doi.org/10.1016/j.physrep.2005.04.001>
46. Thoroddsen, S. T. and Van Atta, C. W. The Influence of Stable Stratification on Small-Scale Anisotropy and Dissipation in Turbulence, *J. Geophys. Res.* **97**, C3, 3647-3658 (1992).

47. Thoroddsen, S. T. and Van Atta, C. W. Experiments on density-gradient anisotropies and scalar dissipation of turbulence in a stably stratified fluid. *J. Fluid Mech.* **322**, 383-409 (1996).
48. Piccirillo, P. and Van Atta, C. W. The evolution of a uniformly sheared thermally stratified turbulent flow. *J. Fluid Mech.* **334**, 61-86 (1997).
49. Keller, K. H. and Van Atta C. W. An experimental investigation of the vertical temperature structure of homogeneous stratified shear turbulence. *J. Fluid Mech.* **425**, 1-29 (2000).
50. Holt, S. E., Koseff, J. R. and Ferziger, J. H. 1992 A numerical study of the evolution and structure of homogeneous stably stratified sheared turbulence. *J. Fluid Mech.* **237**, 499-539.
51. Fernando, H. J. S.; Pardyjak, E. R.; Di Sabatino, S.; Chow, F. K.; De Wekker, S. F. J.; Hoch, S. W.; Hacker, J.; Pace, J. C.; Pratt, T.; Pu, Z. et al. The MATERHORN –unraveling the intricacies of mountain weather. *Bull. Am. Meteorol. Soc.* **96 (11)**, 1945–1967 (2015).
52. Kit, E.; Hocut, C.; Liberzon, D. and Fernando, H.J.S. Fine-Scale Turbulent Bursts in Stable Atmospheric Boundary Layer in Complex Terrain. *J. Fluid Mech.* **833**, 745-772 (2017).
53. Sukoriansky, S.; Kit, E.; Zemach, E.; Midya, S. and Fernando, H.J.S. Inertial range skewness of the longitudinal velocity derivative in locally isotropic turbulence. *Phys. Rev. Fluids* **3**, 114605 (2018).
54. Batchelor, G. K. and Townsend, A. A. Decay of vorticity in isotropic turbulence. *Proc. R. Soc. London A* **190**, 534-550 (1947).
55. Kit, E.; Cherkassy, A.; Saint, T.; Fernando, H. J. S. In-situ calibration of hot-film probes using a co-located sonic anemometer: implementation of a neural network. *J. Atmos. Ocean Tech.*, **27**, 23-41 (2010).
56. Conry, P.; Kit, E.; Fernando, H. J. S. Measurements of mixing parameters in atmospheric stably stratified parallel shear flow. *Environ. Fluid Mech.* **20**, 1177–1197 (2020).
57. Kurien, S., Sreenivasan K. R. “Measures of anisotropy and the universal properties of turbulence,” in *New Trends in Turbulence: Nouveaux Aspects*, edited by M. Lesieur, A. Yaglom, and F. David, (Springer, Berlin, 2001), pp. 53–111.